frontiers in Materials

ORIGINAL RESEARCH
published: 16 November 2020
doi: 10.3389/fmats.2020.580424

High-Performance Supercapacitor Electrode Obtained by Directly Bonding 2D Materials: Hierarchal MoS_2 on Reduced Graphene Oxide

Mutawara Mahmood Baig[1], Erum Pervaiz[1], Minghui Yang[2] and Iftikhar Hussain Gul[1]*

[1]School of Chemical and Materials Engineering (SCME), National University of Sciences and Technology (NUST), Islamabad, Pakistan, [2]Solid State Functional Materials Research Lab (SSFMRL), Ningbo Institute of Materials Technology and Engineering (NIMTE), Chinese Academy of Science (CAS), Ningbo, China

Energy storage devices are the ultimate flexible solution to overcome energy deficiency. Thre is a need is to find innovative nanomaterials to overcome the delays in efficiency and sustainability. Herein, we report the synthesis of hierarchical MoS_2/rGO nanohybrids as electrode material for supercapacitors. Pure phase and flower-shaped molybdenum disulfide (MoS_2) nanosheets have been synthesized using a meek hydrothermal method followed by the preparation of MoS_2/rGO nanohybrids. The physicochemical aspects and electrochemical properties have been carefully analyzed using cyclic voltammetry and galvanostatic charge-discharge method in the 1 M KCL electrolyte. The capacitance of MoS_2 and MoS_2/rGO were found to be 297 F/g (66 mAh/g or 238 C/g) and 850 F/g (153.5 mAh/g or 552.5 C/g) at 1 A/g respectively, with 95.3% retention in capacitance after 10,000 cycles at 2 A/g. The improved electrochemical performance of the MoS_2/rGO electrode could be ascribed to rapid diffusion pathways delivered by rGO and improved redox reactions of hierarchical MoS_2 nanosheets owing to the high surface area (391 m^2/g). This feature enables a decrease in the entire impedance of electrodes which agrees with the findings obtained from electrochemical impedance spectroscopy.

Keywords: rGO, MoS_2, 2D materials, supercapacitors, energy storage

OPEN ACCESS

Edited by:
Mohammad Islam,
King Saud University, Saudi Arabia

Reviewed by:
Gang Zhao,
University of Jinan, China
Xing-Long Wu,
Northeast Normal University, China

****Correspondence:***
Erum Pervaiz
erum.pervaiz@scme.nust.edu.pk

Specialty section:
This article was submitted to Energy Materials, a section of the journal Frontiers in Materials

Received: *06 July 2020*
Accepted: *26 August 2020*
Published: *16 November 2020*

Citation:
Baig MM, Pervaiz E, Yang M and Gul IH (2020) High-Performance Supercapacitor Electrode Obtained by Directly Bonding 2D Materials: Hierarchal MoS_2 on Reduced Graphene Oxide. Front. Mater. 7:580424. doi: 10.3389/fmats.2020.580424

HIGHLIGHTS

- The hierarchical MoS_2/rGO nanohybrids have been synthesized for supercapacitors.
- Pure phase and flower shaped MoS_2 nanosheets have been synthesized using a mild hydrothermal method.
- The electrode showed a high specific capacitance of 850 F/g.
- The electrode exhibited 95.3% retention in capacitance after 10,000 cycles at 2 A/g.
- The electrochemical impedance revealed low resistance (0.325 Ω) as well as a small frequency response (2.778 s).

INTRODUCTION

Pseudo-capacitors being an important class of supercapacitors are widely employed for efficient energy storage. They have attracted great scientific and technical attention owing to the possible

integration of the benefits of lithium-ion batteries (high energy density) and capacitors (high power density). Their capability to undergo rapid and reversible redox reactions made them a strong candidate to accumulate charges as compared to double-layer capacitors (Winter and Brodd, 2004; Tang et al., 2015; Binazadeh et al., 2016; Ghosh et al., 2019; Lv et al., 2019; Miao et al., 2019; He et al., 2020). However, the energy density of most commercially available electrochemical capacitors is much lower than that of lithium-ion batteries, creating a substantial barrier to the practical application of such supercapacitors on a large scale (Jabeen et al., 2017; Liu et al., 2018a; Zhao et al., 2018). The energy density depends on the capacitance and the potential window by relation $E = ½CV^2$. Therefore, considerable efforts have been made to maximize "E" by enhancing "V" and "C." Among various types of electrochemical capacitors, 2D materials-based supercapacitors like graphene and MoS_2, are gaining significant interest because of their intrinsic features, such as their high conductivity, low cost, flexibility, wide potential, window and fast redox reaction (Firmiano et al., 2014; Hao et al., 2014; Sun et al., 2015; Lv et al., 2016; Mehran and Baig, 2019; Muthu and Gopalan, 2019; Khan et al., 2020; Rani et al., 2020; Rathinamala et al., 2020; Zhao et al., 2021).

Molybdenum disulfide has been widely investigated for various applications such as catalysis (electrocatalysis and photocatalysis) for H_2 production, sensors, lubricating agents, transistors, and electrode materials for rechargeable batteries (Chhowalla and Amaratunga, 2000; Chen et al., 2001; Sun et al., 2004; Murugan et al., 2006; Chakraborty et al., 2012; Firmiano et al., 2012; Wang et al., 2012). As a distinctive layered sulfide of a transition metal, MoS_2 is comprised of three atomic layers (S-Mo-S), which are stacked on top of each other and connected through "Van der Waals" forces (Geim and Grigorieva, 2013; Molina-Sánchez et al., 2015). This flexibility is because of its 2D nature, which is analogous to the graphene (Matte et al., 2010). Numerous approaches have been made to produce MoS_2, such as the hydrothermal method (Chang and Chen, 2011b), thermal evaporation-exfoliation (Balendhran et al., 2012), physical vapor deposition (Lee et al., 2012), chemical vapor deposition (Shaw et al., 2014), chemical exfoliation (Sadan et al., 2008), mechanical exfoliation (Zhou et al., 2011), and wet chemical approaches (Altavilla et al., 2011). However, during the synthesis process, these methods led to the formation of buckyball-like nanoparticles or nanotube of MoS_2 (Rosentsveig et al., 2001; Rapoport et al., 2005). An effective way to resolve this issue and to get the layered structured MoS_2 is to employ carbon materials such as graphene, as a template (Chang and Chen, 2011; Hwang et al., 2011; Li et al., 2011; Wang et al., 2018; An et al., 2019; Li et al., 2019b). The graphene impedes the formation of three dimensional MoS_2, resulting in the 2D growth of MoS_2 on graphene nanosheets during the synthesis process (Chang and Chen, 2011a; Hwang et al., 2011; Li et al., 2011). Moreover, besides the elemental support of the graphene during the synthesis process, the coupling effects among MoS_2 and graphene could create a hybrid material with unique characteristics. These coupling effects are controlled by nature of chemical bonds among these materials (Xu et al., 2020; Yang et al., 2020; Zhao et al., 2020). MoS_2 could hypothetically store charges in three ways: 1) "intersheet" and 2) "intrasheet" double layer storage on single atomic layers by diffusion process, or 3) the faradic redox process on a molybdenum center, as molybdenum possess numerous oxidation states (+2 to +6), making it an ideal pseudocapacitive material, like RuO_2 (Soon and Loh, 2007). However, MoS_2 has a stumpy specific capacitance which might be attributed to its low electric conductivity. Recently, Yun Lu et al. demonstrated that this issue could be resolved using FeS_2@ carbon as a template for synthesis of MoS_2. Based on the same approach, graphene could be employed as a substrate to grow MoS_2. Graphene oxide could act as an ideal template for the growth of MoS_2 to enhance its electrochemical properties due to excellent electric conductivity, high surface area, and stability, which provides excessive ion diffusion pathways among MoS_2 and electrolyte interfaces. Another way to improve the performance of supercapacitors is using the element doping strategy (Ghosh et al., 2020; Wang et al., 2020a). For example, Wang et al. (2020b) employed the strategy of multivalent and isostructural anion substitution chemistry to enhance the electrochemical performance of electrode materials.

Herein, we have fabricated hierarchal MoS_2 flowers on GO sheets using a simplistic hydrothermal scheme, and prepared hybrid nanostructures are employed as potential electrode materials for supercapacitor applications. We observed that the MoS_2 layers grown on rGO retain highly efficient charge storage properties with excessive capacitance and energy density properties. The remarkable capacitive performance of the MoS_2/rGO hybrid electrode is likely due to the integration of faradic and non-radical processes of active MoS_2 layers in connection with highly conductive graphene oxide layers.

EXPERIMENT

Fabrication of Pure MoS_2 and MoS_2/rGO Nanohybrids

For the preparation of pure MoS_2 and its hybrid with reduced graphene oxide, a facile hydrothermal method is adopted with prior ultrasonication treatment. Analytical grade ammonium heptamolybdate $(NH_4)_6Mo_7O_{24}$, thiourea (CH_4N_2S), polyvinyl pyrrolidone (PVP, K30, Mol. wt. 40,000) $(C_6H_9NO)_n$, graphite flakes, sulfuric acid, sodium nitrate, potassium permanganate and acetic acid (CH_3COOH) were used as received. Graphene oxide was synthesized by a modified Hummers method (Xu et al., 2008; Zhu et al., 2011). Prior to the reaction in a Teflon-lined autoclave, 30 mg GO was suspended in 50 ml water using probe sonication for 2 h. 10 mmol CH_4N_2S was added in GO suspension with continuous stirring for 20 min. A further 5 mmol $(NH_4)_6Mo_7O_{24}$ was dissolved in 25 ml water at ambient conditions, followed by the addition of 150 mg PVP. Both the solutions (GO suspension and AHM solution) were mixed, keeping the temperature to a low value using an ice bath, and subjected to ultrasonication for 30 min. Just before the transfer of the mixture to autoclave, 1.5 ml CH_3COOH was added to the mixture. The autoclave was kept in an oven at 180°C for 16 h. Later, black precipitates were filtered, washed using ethanol and water repeatedly, and dried at 80°C for 8 h. For pure MoS_2, same procedure is adopted but in the absence

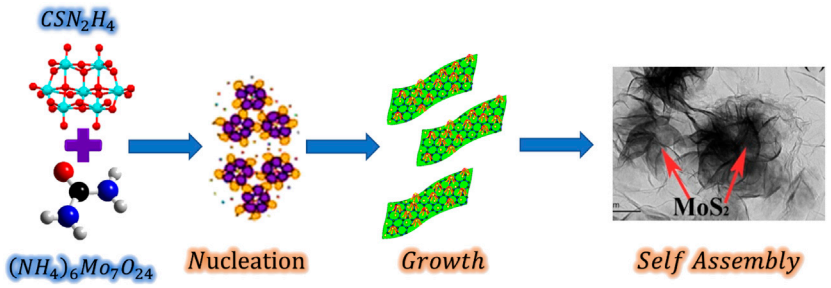

FIGURE 1 | Schematic illustration of the morphological evolution process of the 3D flower-like MoS_2 on rGO.

of GO. After that, the Ni foam substrates (1 × 1 cm^2) were treated with a 3 M HCl solution followed by washing and drying at 60°C overnight. The powered electrode materials were drop cast on pre-treated Ni foam by making an ink (10 mg of powder in a mixture of 500 µL DI water, 450 µL isopropanol, and 50 µL Nafion, followed by 1 h sonication) until the desired mass loading was achieved. After deposition, Ni foam was dried overnight at 80°C.

Electrodes Physicochemical Measurements

Phase analysis was carried out by powder X-ray diffraction ("STOE-Seifert X'Pert PRO") using "CuKα" radiation at 2θ values from 10° to 80°. The morphology of electrodes was examined using scanning electron microscopy ("JEOL-instrument JSM-6490 A") and transmission electron microscopy. The electrochemical testing was executed at an ambient temperature by "VMP3 multi-channel potentiostat/galvanostat." For the three-electrode system, MoS_2, and MoS_2/rGO were employed as a working electrode, Ag/AgCl was used in 1 M KCl solution for the reference electrode, and a platinum mesh was used as a counter electrode. Cyclic voltammetry was executed at different scan rates (2–50 mV/s). Galvanostatic charge-discharge was performed at various current densities (1–10 Ag^{-1}). Electrochemical impedance spectroscopy was accomplished at 5 mV in the frequency range from 0.1 Hz to 100 kHz.

RESULTS AND DISCUSSION

Physicochemical Characterization

To elucidate the growth mechanism of hierarchical MoS_2 flowers, a schematic diagram is presented in **Figure 1**. The growing mechanism is consistent with preceding literature (Burda et al., 2005; Zhang et al., 2015) of the "three-stage growth" mechanism, which includes rapid nucleation of amorphous primary particles, oriented aggregation of nanosheets, and self-assembly of hierarchical structures. Hydrolysis of thiourea to H_2S leads to the formation of the MoS_2 nuclei that consequently grows into nanosheets corresponding to their crystal growth tendency. When many nuclei were synthesized, it could result in the reduction of nutrients in the reaction medium for endowing formation of MoS_2 nuclei, and subsequent reduction of nanosheets in dimensions. Afterward, these nanosheets intertwined and rolled longitudinally to create flower-like nanospheres, constrained by the lowering of surface energy. The succeeding chemical reactions (**Eqs 1-4**) were proposed to have occurred throughout the entire transition progression (Nagaraju et al., 2007; Feng et al., 2009; Ma et al., 2013; Sun et al., 2014; Zhang et al., 2015; Sun et al., 2016)

$$CSN_2H_4 + 2H_2O \rightarrow 2NH_3 + CO_2 + H_2S \quad (1)$$

$$(NH_4)_6Mo_7O_{24} \rightarrow 6NH_3 + 7MoO_3 + 3H_2O \quad (2)$$

$$MoO_3 + 3H_2S + 2H_2O \rightarrow MoO_2 + SO_4^{2-} + 2H^+ \quad (3)$$

$$MoO_2 + 2H_2S \rightarrow MoS_2 + 2H_2O \quad (4)$$

The crystal structure and phase purity of synthesized nanomaterials were examined using X-ray diffraction. As displayed in **Figure 2A**, diffraction peaks located at 2θ = 14.2, 33.5, 40.2, 49.3, 58.9, and 69.5 were evident in both patterns of bare MoS_2 and MoS_2/rGO nanohybrids, which are well indexed to (d_{002}), (d_{100}), (d_{103}), (d_{105}), (d_{110}), and (d_{201}) crystal planes of hexagonal phase MoS_2 (JCPDS no. 37-1492). The well-broadened peaks could be ascribed to a lesser thickness of MoS_2 nanomaterial, confirming poor crystallinity of the MoS_2 nanomaterial and more defects with decreased nanometer-scale sizes. **Figure 2B** presents the nitrogen adsorption desorption isotherms for both pure MoS_2 and MoS_2/rGO hybrids. Adsorption isotherms depict type-II adsorption behavior, representing a multilayer adsorption taking place on the surface of both samples. A long plateau before saturation represents multilayer adsorption till it reaches maximum near the saturation pressure. The calculated multipoint BET analysis showed that the specific surface area of MoS_2/rGO nanohybrids was found to be 391 m^2/g, which is a significantly higher value as compared to pure MoS_2 (124 m^2/g). The resulting pore size-distribution exhibits manifestation of abundant mesopores, as shown in **Figure 2C**. The porous structure is advantageous for fast electrolyte diffusion and mass transportation. The average pore size of pure MoS_2 was 24 Å, while for those of MoS_2/rGO (average pore size 58 Å) an increment of 24 Å in pore size was seen, whereas the pore volume for pure MoS_2 was 0.08 cm^3/g and pore volume for

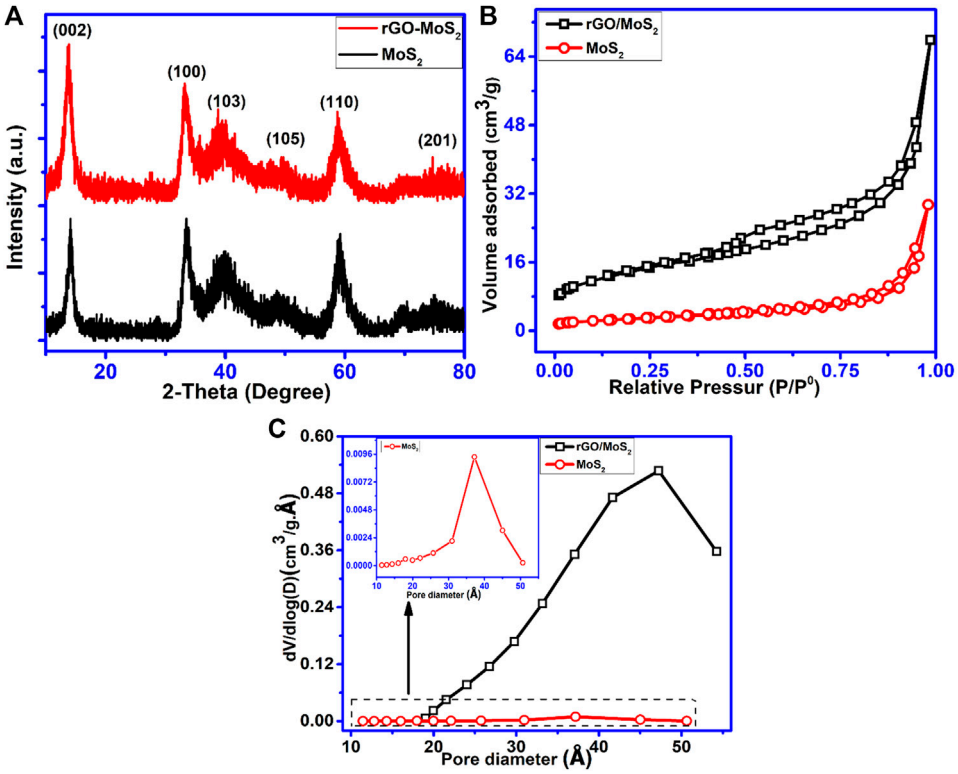

FIGURE 2 | (A) XRD patterns of pure MoS_2 and MoS_2/rGO. **(B)** BET N_2 adsorption-desorption isotherms for pure MoS_2 and MoS_2/rGO nanocomposites. **(C)** Pore volume and pore size distribution for pure MoS_2 and MoS_2/rGO nanocomposites.

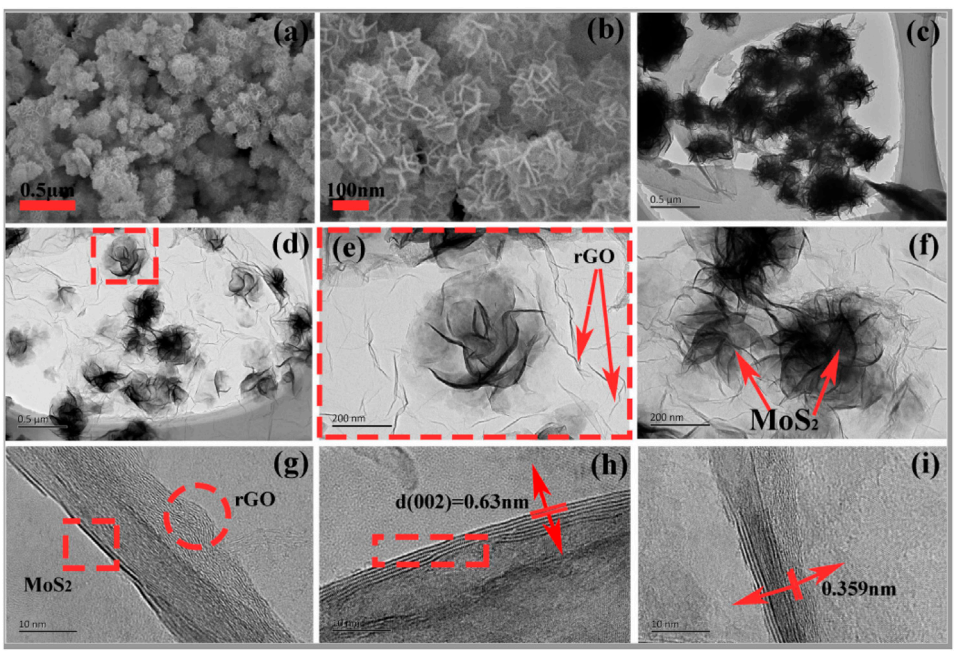

FIGURE 3 | (A,B) SEM images of pure MoS_2 **(C)** TEM images of pure MoS_2 **(D–I)** TEM images of MoS_2/rGO nanocomposite.

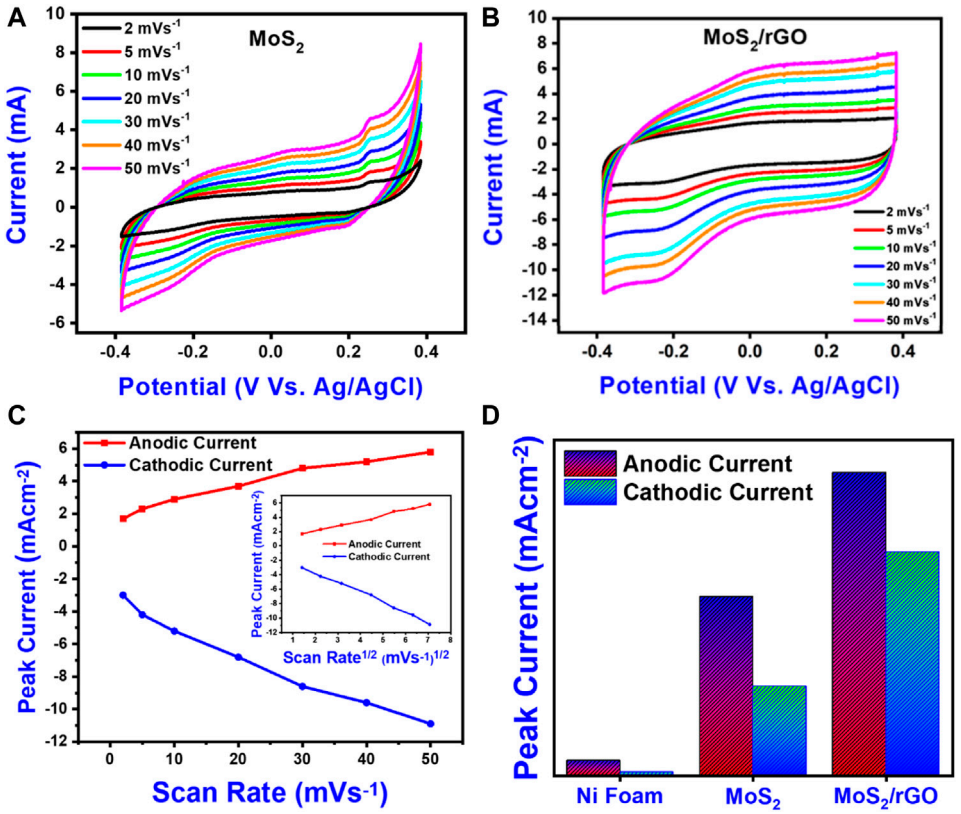

FIGURE 4 | Electrochemical performance of as-synthesized electrodes in a three-electrode configuration. **(A)** CV curves of MoS_2 on Ni foam. **(B)** CV curves of MoS_2/rGO nanocomposite on Ni foam. **(C)** Variation of peak current with scan rate and variation of peak current with square root scan rate (inset) for MoS_2/rGO nanocomposite on Ni Foam. **(D)** Histogram of different electrode materials.

MoS_2/rGO was found to be 0.347 cm^3/g. The increase in pore size is presumably because of gaps among MoS_2/rGO nanosheets as evident from the SEM images. SEM images (**Figures 3A,B**)) display the flower-like morphology of the resulting MoS_2 nanosheets containing hundreds of curved MoS_2 nanosheets, leading to hierarchical flowers. These hierarchical flowers possess a diameter of 115 nm and a thickness of 3.42 nm without agglomeration. These nanosheets are tangled together, causing many voids between them due to their curved morphology. Such small-sized nanoflowers provide abundant edge sites for MoS_2 nanosheets. Based on the growth mechanism, it can be inferred that thiourea is disintegrated to sulfur ions and fastened on the surface of rGO via nucleation, forming the MoS_2 nanoflower that entirely overlays all surfaces of rGO. **Figure 3C** shows the TEM image of MoS_2 while **Figures 3D–I** shows MoS_2 wrapped by rGO sheets, forming a 2D-2D network. TEM images revealed that MoS_2 nanosheets were completely *in-situ* anchored on rGO, which provides cross-linking with MoS_2 developing a well-interconnected network. Moreover, MoS_2 nanosheets were a few layers thick, and the void among layers was 0.63 and 00.36 nm for MoS_2/rGO, which corresponds with d-spacing of 0.63 nm (002), estimated by X-ray diffraction. Extended interlayer spaces are extremely advantageous in enhancing the kinetic capability of rapid and reversible intercalation/deintercalation of anions. The fringes twisted from the straight track could be elucidated as lattice defects in MoS_2 and rGO. These defects have the capacity for more electrolyte ions which might improve all electrochemical properties by delivering enough electroactive sites and extra electrical conductivity. This 2D-2D architecture is also advantageous to enhance the surface area of the nanocomposite. Moreover, the overlapping or merging of rGO creates an interrelated conducting framework and aids in fast electron transportation during a redox reaction. This 2D-2D nanostructure also improves the stability of MoS_2/rGO composites owing to the flexibility and toughness of rGO.

Electrochemical Measurements

CV profiles of MoS_2 and MoS_2/rGO on Ni foam evaluated in scan rates from 2 mVs^{-1} to 50 mVs^{-1} are presented in **Figures 4A,B**. Cyclic voltammograms revealed a combination of rectangular (double-layer reaction) and redox peaks indicating the pseudocapacitive behavior with a fast-reversible redox reaction of MoS_2. A similar trend can be seen in most of the reported literature (Firmiano et al., 2014; Ji et al., 2015; Liu et al., 2018b; Tian et al., 2019). The CV curves retained their shapes after 50 mV/s, suggesting the good high rate electrochemical properties such as high stability, fast electrolyte ions diffusion

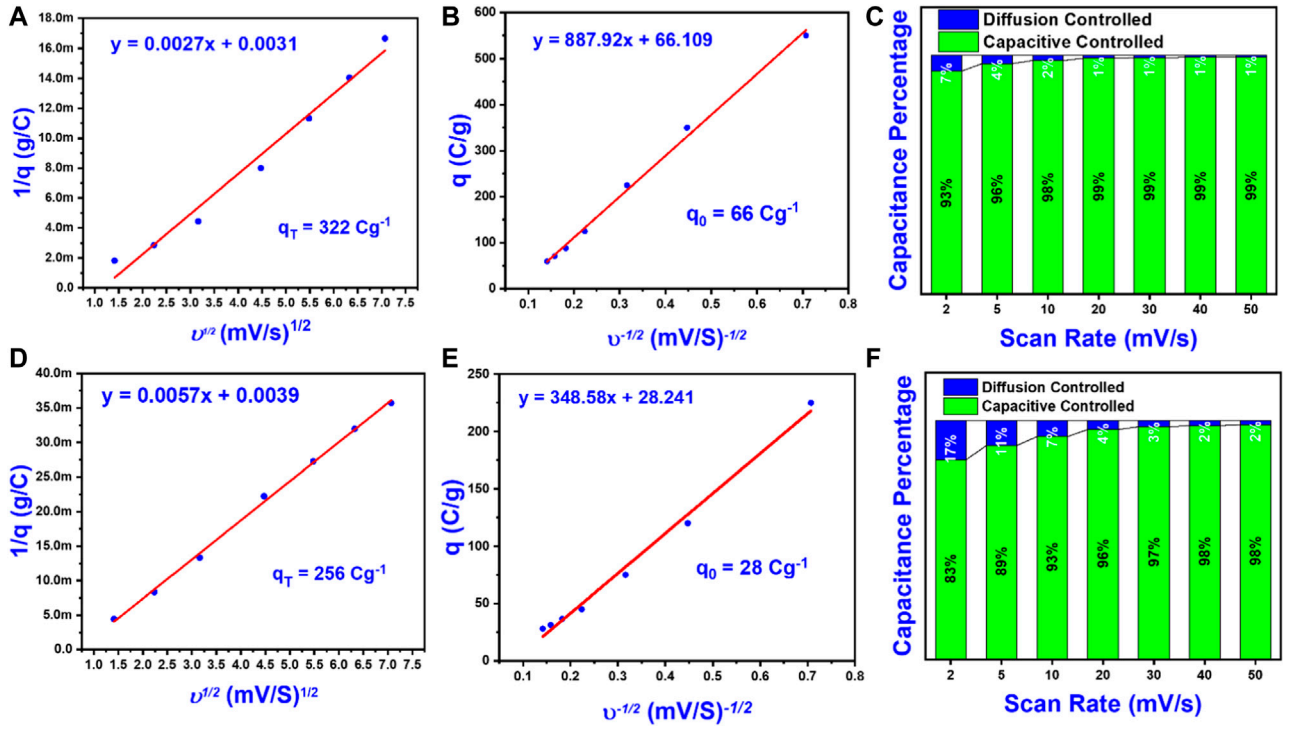

FIGURE 5 | Electrochemical performance of as-synthesized electrodes in a three-electrode configuration. **(A)** The inverse of the charge stored vs. the square root of the scan rate for MoS_2/rGO nanocomposite on Ni Foam. **(B)** The charge stored vs. the inverse of the square root of the scan rate for MoS_2/rGO nanocomposite on Ni Foam. **(C)** The capacity contribution at different scan rates of MoS_2/rGO nanocomposite on Ni Foam. **(D)** The inverse of the charge stored vs. the square root of the scan rate for pure MoS_2 on Ni Foam. **(E)** The charge stored vs. the inverse of the square root of the scan rate for pure MoS_2 on Ni Foam. **(F)** The capacity contribution at different scan rates of pure MoS_2 on Ni Foam.

into the active site, and good reversibility. Moreover, the current density of the MoS_2/rGO electrode has been improved greatly due to the addition of rGO instead of the pure MoS_2 electrode. The enhanced current density could be ascribed to high conductivity and effective utilization of active sites of MoS_2 after the growth on rGO (Tian et al., 2019). The peaks in the CV profiles of MoS_2-based electrodes could be ascribed to the redox reaction of layer structure MoS_2 i.e. Mo-IV ↔ Mo-V ↔ Mo-VI as per the following equations (**Eqs 5 and 6**) (Soon and Loh, 2007; Tian et al., 2019; Sun et al., 2020).

$$(MoS_2)_{Surface} + K^+ + e^- \leftrightarrow (MoS_2 - K^+)_{Surface} \quad (5)$$

$$MoS_2 + xe^- + xK^+ \leftrightarrow (MoS - SK) \quad (6)$$

The non-faradic process is ascribed to the adsorption and desorption of electrolyte ions (K^+ ions) on the surface and intrasheet/intasheet of MoS_2 layers. The faradic reaction, on the other hand, is favored by Mo atoms. To further verify the charge storage mechanism and kinetics of oxidation and reduction scan, sweep voltammetry was performed by manipulating CV curves at different scan rates. **Figure 4C** displays a plot of anodic and cathodic peaks current as a function of scan rate with the inset as the square root of the scan rate for MoS_2/rGo. The peak current is determined using "Randles–Sevcik Equation (**Eq. 7**)" (Sarkar et al., 2018)

$$i_P = 0.4961\, nFAC\left(\frac{nFvD}{RT}\right)^{\frac{1}{2}} \quad (7)$$

where "*n*" is the number of electrons transferred, "i_p"$_P$ is peak current, "*F*" is Faraday constant, "*A*" electrode area, "*C*" is ions concentration, "*D*" is diffusion coefficient; and "*v*" represents scan rate. For the non-diffusion controlled process, the trend among scan rates and peak currents should be a straight line (Hu et al., 2009). **Figure 4C** shows a non-linear relation among scan rates and peak currents, indicating a diffusion-controlled process instead of a non-diffusion process (Hu et al., 2009). For comparative study, peak currents were independently sketched in **Figure 4D** which showed that both cathodic and anodic current was highest for MoS_2/rGO. However, the anodic current is higher as compared to the cathodic current, which could be due to the kinetic limitations of K+ ions over electrons (Kulkarni et al., 2014). rGO allows effective intercalation/de-intercalation of K+ ions by delivering additional conductive paths, ensuring a fast transference of charges through the interface which enhances all electrochemical properties (Gopalakrishnan et al., 2015). The specific capacitance "C_s" was computed by the equation below (**Eq. 8**) from CV curves (Kim et al., 2013)

$$C_s = \frac{\int idV}{2mV_s\Delta V} \quad (8)$$

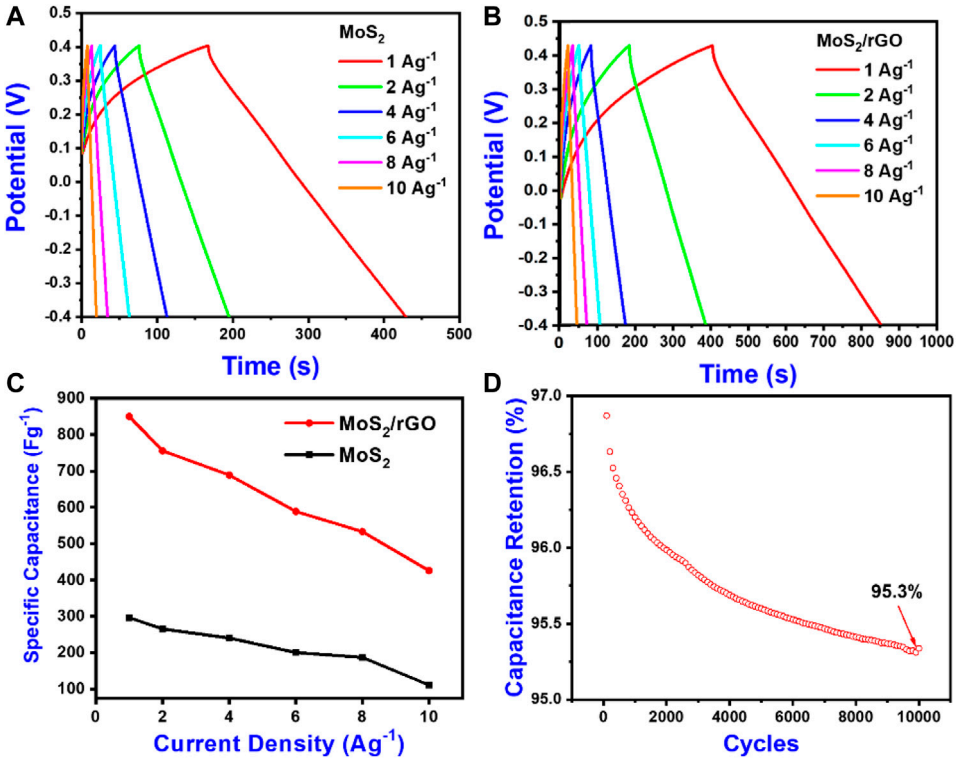

FIGURE 6 | Electrochemical performance of as-synthesized electrodes in a three-electrode configuration. **(A)** Galvanostatic charge-discharge curves of pure MoS_2 on Ni Foam. **(B)** Galvanostatic charge-discharge curves of MoS_2/rGO nanocomposite on Ni Foam. **(C)** Gravimetric capacitance from GCD curves as a function of scan rate for MoS_2/rGO nanocomposite and MoS_2 on Ni Foam. **(D)** Cyclic stability of MoS_2/rGO nanocomposite measured at 2 A/g.

Where "$\int idV$" is the integral area under the CV curve," "m is the active mass of electrode material, "V_s" is the scan rate, and "ΔV" is the potential window. The maximum capacitance of MoS_2 and MoS_2/rGO were found to be 281 F/g (62.5 mAh/g or 225 C/g) and 846 F/g (153 mAh/g or 550 C/g) at 2 mV/s, respectively.

"Trasatti method" was applied for exploring the electrochemical kinetics of active materials and processes through which charges are stored in electrodes (Ardizzone et al., 1990). This analysis relies on computing stored, charges precisely on external and internal surfaces of electrodes. The overall amount of charges stored is the sum of both surfaces' charges stored as per the following equation (**Eq. 9**)

$$q_T = q_i + q_o \tag{9}$$

Where q_T is total charges and q_o and q_i are charges on external and internal surfaces. The amount of charges on the external surface is an adsorption mechanism and does not depend on the scan rate. Whereas, at the internal surface, the quantity of charges is a "diffusion-controlled" mechanism. Therefore, the overall volumetric charges are dependent on scan rates as per the equation mentioned in our previous report (Baig et al., 2020). **Figure 5** showed the plot between scan rates and the quantity of charges stored on the surface. From **Figures 5A,D** overall charges "q_T" could be estimated after the extrapolation of scan rates to zero, whereas "q_o" could be estimated after extrapolation of scan rates to infinity as shown in **Figures 5B,E**. **Figured 5C,F** showed capacitive (surface effects) and adsorption contributions of MoS_2/rGO and pure MoS_2 electrodes at various scan rates. The estimated capacitive contributions are significantly greater than a diffusion-controlled contribution at the same scan rates, demonstrating the highly efficient surface storage. The total charge contribution of the composite electrode was around 322 C/g, which is approximately 1.3 times greater than the pure MoS_2 electrode. Furthermore, the MoS_2/rGO electrode showed the capacitive contribution of 99% slightly increased from the MoS_2 counterpart, which accounts for 98% capacitive contribution. This means that most of the surfaces are fully accessible to electrolyte ions during the charge/discharge processes due to the increased interlayer spacing of MoS_2 layers resulting from the prevention of restacking of MoS_2 layers in the MoS_2/rGO electrode (Yan et al., 2017). The enhanced performance of the composite electrode could be attributed to high conductivity and efficient use of active sites of MoS_2 after the growth on rGO. Moreover, by increasing the scan rates, the diffusion-controlled process decreases due to a remarkable decline in ions' diffusion time into the lattice, resulting in low overall capacity at high scan rates (Yan et al., 2017; Jiang et al., 2018).

GCD analysis was executed to authenticate the rate capabilities of electrode materials at current densities from 1 A/g to 10 A/g and is presented in **Figure 6**. **Figures 6A,B** signifies the GCD

TABLE 1 | Specific capacitance of MoS_2-based electrodes reported by different groups.

Sr no	Material	Year	Electrolyte	Capacitance (F/g)	Cyclic stability	Ref
1	MoS_2/rGO	2016	2M KOH	218	91.88% retention after 1,000 cycles	(Xiao et al., 2016)
2	MoS_2/Graphene	2013	1M Na_2SO_4	243	92.3% retention after 1,000 cycles	(Huang et al., 2013)
3	MoS_2/rGO	2014	1M $HCLO_4$	265	92% retention after 1,000 cycles	(Firmiano et al., 2014)
4	MoS_2/rGO	2019	—	331	110.7% retention after 15,000 cycles	(Li et al., 2019a)
5	MoS_2/Graphene	2016	1M Na_2SO_4	410	80.3% retention after 10,000 cycles	(Sun et al., 2016)
6	MoS_2/Graphene	2020	1M Na_2SO_4	428	88% retention after 5,000 cycles	(Sun et al., 2020)
7	MoS_2/rGO	2018	1M KOH	440	83% retention after 1,400 cycles	(Raghu et al., 2018)
8	MoS_2/PANI/rGO	2016	1M Na_2SO_4	618	96% retention after 2,000 cycles	(Sha et al., 2016)
9	MoS_2/Graphene	2019	1M KOH	756	88% retention after 10,000 cycles	(Vikraman et al., 2019)
10	MoS_2/rGO	2015	PVA/H_2SO_4	5.2 F/cm^3	99.9% retention after 7,000 cycles	(Sun et al., 2015)
11	MoS_2/rGO	2020	1M KCl	850	95.3% retention after 10,000 cycles	This work
12	1T-MoS_2	2019	3M KOH	1,120	96% retention after 2,000 cycles	(Wei et al., 2019)

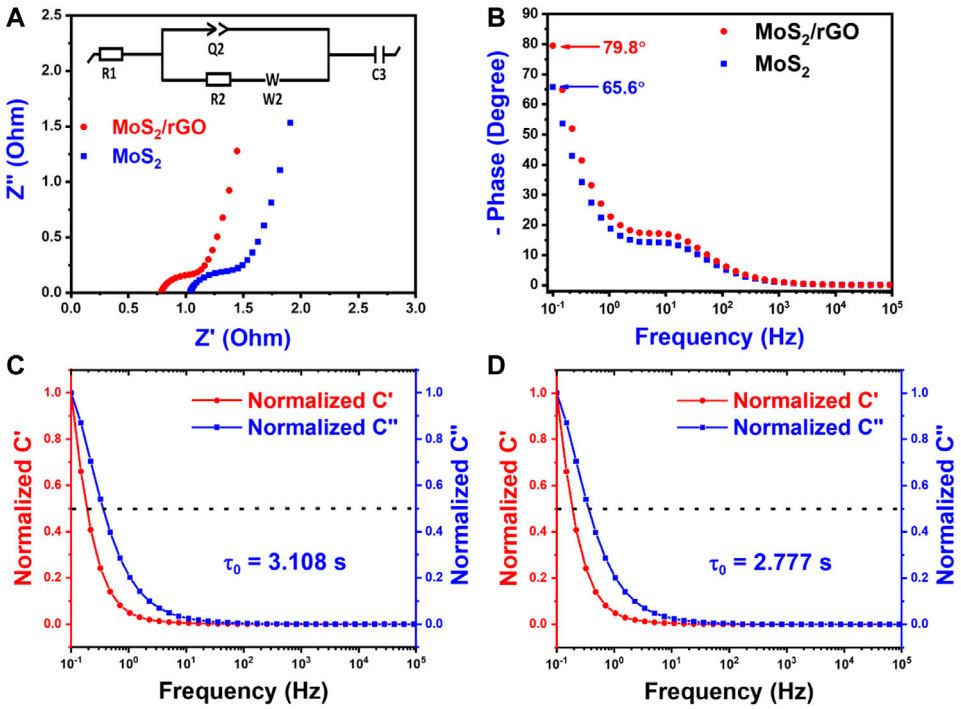

FIGURE 7 | Electrochemical performance of as-synthesized electrodes in a three-electrode configuration. **(A)** Nyquist plot of MoS_2/rGO nanocomposite and MoS_2 on Ni foam. **(B)** Bode phase angle plot of MoS_2/rGO nanocomposite and MoS_2 on Ni foam. **(C)** Normalized real and imaginary capacitance vs. frequency of MoS_2 on Ni foam. **(D)** Normalized real and imaginary capacitance vs. frequency of MoS_2/rGO nanocomposite on Ni foam.

profile of MoS_2 and MoS_2/rGO (vs Ag/AgCl) at 1–10 A/g. The MoS_2/rGO/Ni has a remarkably higher discharge time (459 s) as compared to its counterpart, which has a discharge time of 266 s at 1 Ag^{-1}. The GCD analysis shows that, with the increase in current densities, discharge time decreases. This is because electrochemical kinetics could not cope with fast fluctuations in potential because of the sluggish transport of ions and ineffective utilization of active materials (Azad et al., 2020; Zhao et al., 2020). The charging profiles are nearly straight and identical to the discharge counterparts, which again reveals the outstanding reversibility of the MoS_2/rGO electrode. The Ohmic drop ("IR drop" or "ESR") is insignificant even at greater current densities, demonstrating the exceptional electronic conductivity of electrodes. This low "Ohmic drop" could be because of the rapid intercalated/deintercalated phenomena of K^+ and fast electrons transfer. In comparison, both capacitance (F/g) and capacity (mAh/g and C/g) were used. The maximum capacitance of MoS_2 and MoS_2/rGO was found to be 297 F/g (66 mAh/g or 238 C/g) and 850 F/g (153.5 mAh/g or 552.5 C/g) at 1 A/g respectively, and are presented in **Figure 6C**. The rate capability of MoS_2/rGO can be attributed to the increased interlayer spacing caused by the incorporation of rGO nanosheets in between MoS_2 layers while maintaining its good conductivity. These characteristics further improve the diffusion and transportation of electrolyte ions and increase the surface area accessible to the electrolyte ions. **Table 1**

TABLE 2 | Equivalent circuit parameters of as-synthesized electrodes.

Electrode material	R_1 (Ω)	Q_2 ($F.s^{(a-1)}$)	a_2	R_2 (Ω)
MoS_2/rGO	0.785	0.088	0.819	0.325
MoS_2	1.089	0.159	1.548	0.654

presents the evaluation of capacitance from previously reported literature. **Figure 6D** showed the stability test of MoS_2/rGO was executed by periodic galvanostatic charge-discharge cycles for 10,000 cycles at 2 A/g. The MoS_2/rGO nanocomposite exhibited an excellent capacity retention of 95.3% after 10,000 cycles, whereas the MoS_2 exhibited a retention rate of only 79.4%. The excellent cyclic stability of the composite electrode is the direct result of the excellent mechanical and chemical properties of rGO. This might also be a result of the substrate which helps in sustaining the electrode structure and conductivity by having good compatibility with the electrolyte.

Electrochemical impedance spectroscopy was employed to assess charging kinetics in relation to capacitive behavior. **Figure 7A** shows the Nyquist plot of synthesized electrodes. The inset in **Figure 7A** presents the equivalent circuit elements (Azad et al., 2020), where "R_1" is the ohmic resistance of the solution between the working and reference electrode, "R_2" is the polarization or the charge transfer resistance at the electrode and solution interface, "Q_2" is the constant phase element at this interface, "W_2" is Warburg impedance, and "C_3" is the faradic capacitance. Usually, a semi-circle (dia of this circle gives R_{ct}) could be observed in the "Nyquist plot" at higher frequencies, because of charge transfer resistances caused by faradic reactions. The R_{ct} values were 0.6542 and 0.3256 Ω for MoS_2 and MoS_2/rGO respectively (**Table 2**). The solution resistances for the MoS_2 and MoS_2/rGO were 1.089 and 0.785 Ω, respectively. The sudden ascend in impedance from the imaginary axis can be observed at the middle frequencies zone. This sudden rise gives "Warburg impedance" which is inclined at 45°, demonstrating a pseudo capacitance nature. The bode plot of MoS_2 and MoS_2/rGO is presented in **Figure 7B**. The impedance features of the supercapacitor fall among ideal resistors (phase angle 0°) and ideal capacitors (phase angle 90°) (Azad et al., 2020; Baig et al., 2020). The phase angle for MoS_2/rGO and MoS_2 was 79.8° and 65.6°, representing the outstanding pseudocapacitance performance of active materials. The charge storage mechanisms were additionally verified via normalize $C'(\omega)$ and $C''(\omega)$ responses as function of frequencies (**Figures 7C,D**) by means of a complex capacitance model (Jiang et al., 2018). The relaxation time for the MoS_2 electrode is 3.108 s, whereas for MoS_2/rGO the relaxation time is 2.778 s, demonstrating the fast frequency response and ion diffusion of the MoS_2/rGO. The electrochemical performance of synthesized electrodes is summarized in **Table 3**.

CONCLUSION

The hierarchical MoS_2/rGO nanohybrids have been synthesized using a facile wet chemical approach as a potential electrode material for supercapacitor applications. The results revealed that the hierarchical nanohybrids have a significantly higher capacitance as compared to their single counterparts. The MoS_2/rGO electrode exhibit maximum capacitance of 850 F/g at 1 A/g, with capacitive retention of 95.3% after 10,000 cycles at a current density of 2 A/g. Furthermore, the electrochemical impedance revealed low resistance (0.325 Ω) as well as small frequency response (2.778 s) for the MoS_2/rGO electrode. rGO enhanced the electrochemical performance by offering conductive routes and excellent mechanical stability. The unusual synergistic effect in such a hybrid electrode is responsible for the efficient electron transfer process. The excellent performance of MoS_2/rGO is ascribed to the inherent electrochemical activity of individual rGO and MoS_2 by developing efficient boundaries among the two phases. The hierarchical 3D network supported on the NF substrate is also effective for exposure of numerous active sites, and thus, boosting the electrons/mass transference.

TABLE 3 | Summary of the electrochemical performance of synthesized electrodes.

Samples	Performance					
	Capacitance	Capacity	Capacity	R_1	R_2	τ_o
	F/g	C/g	mAh/g	Ω	Ω	s
MoS_2	297	238	66	1.089	0.654	3.108
MoS_2/rGO	850	552.5	153.5	0.785	0.325	2.778

DATA AVAILABILITY STATEMENT

All datasets presented in this study are included in the article.

AUTHOR CONTRIBUTIONS

EP: Conceptualization, Supervision, Administration, Resources, Reviewing, and Editing. MB: Methodology, Investigation, Formal analysis, Writing- Original draft preparation, Validation, Data Curation. MY, and IG: Reviewing and Editing.

ACKNOWLEDGMENTS

Author EP would like to acknowledge HEC Pakistan for the financial grant 2017/HEC/NRPU/10482. MY would like to thank the National "Thousand Youth Talents" program of China and Ningbo 3315 program for the support. Author MB would like to acknowledge Indigenous Ph.D. fellowships for 5000 scholars, Higher Education Commission (HEC) Islamabad Pakistan (Phase-II Batch-V) for providing support for this work.

REFERENCES

Altavilla, C., Sarno, M., and Ciambelli, P. (2011). A novel wet chemistry approach for the synthesis of hybrid 2D free-floating single or multilayer nanosheets of MS2@oleylamine (M═Mo, W). *Chem. Mater.* 23 (17), 3879–3885. doi:10.1021/cm200837g

An, Y.-B., Chen, S., Zou, M.-M., Geng, L.-B., Sun, X.-Z., and Zhang, X. (2019). Improving anode performances of lithium-ion capacitors employing carbon-Si composites. *Rare Met.* 38, 1113–1123. doi:10.1007/s12598-019-01328-w

Ardizzone, S., Fregonara, G., and Trasatti, S. (1990). "Inner" and "outer" active surface of RuO_2 electrodes. *Electrochim. Acta.* 35 (1), 263–267. doi:10.1016/0013-4686(90)85068-x

Azad, M., Hussain, Z., and Baig, M. M. (2020). MWCNTs/NiS_2 decorated Ni foam based electrode for high-performance supercapacitors. *Electrochim. Acta.* 345, 136196. doi:10.1016/j.electacta.2020.136196

Baig, M. M., Gul, I. H., Khan, M. Z., Mehran, M. T., and Akhtar, M. S. (2020). Binder-free heterostructured MWCNTs/Al_2S_3 decorated on NiCo foam as highly reversible cathode material for high-performance supercapacitors. *Electrochim. Acta.* 340, 135955. doi:10.1016/j.electacta.2020.135955

Balendhran, S., Ou, J. Z., Bhaskaran, M., Sriram, S., Ippolito, S., Vasic, Z., et al. (2012). Atomically thin layers of MoS_2 via a two step thermal evaporation-exfoliation method. *Nanoscale.* 4 (2), 461–466. doi:10.1039/c1nr10803d

Binazadeh, M., Xu, M., Zolfaghari, A., and Dehghanpour, H. (2016). Effect of electrostatic interactions on water uptake of gas shales: the interplay of solution ionic strength and electrostatic double layer. *Energy Fuels.* 30 (2), 992–1001. doi:10.1021/acs.energyfuels.5b02990

Burda, C., Chen, X., Narayanan, R., and El-Sayed, M. A. (2005). Chemistry and properties of nanocrystals of different shapes. *Chem. Rev.* 105 (4), 1025–1102. doi:10.1021/cr030063a

Chakraborty, B., Bera, A., Muthu, D. V. S., Bhowmick, S., Waghmare, U. V., and Sood, A. K. (2012). Symmetry-dependent phonon renormalization in monolayer MoS_2 transistor. *Phys. Rev. B.* 85 (16), 161403. doi:10.1103/physrevb.85.161403

Chang, K., and Chen, W. (2011a). l-cysteine-Assisted synthesis of layered MoS_2/graphene composites with excellent electrochemical performances for lithium ion batteries. *ACS Nano.* 5 (6), 4720–4728. doi:10.1021/nn200659w

Chang, K., and Chen, W. (2011b). *In situ* synthesis of MoS_2/graphene nanosheet composites with extraordinarily high electrochemical performance for lithium ion batteries. *Chem. Commun.* 47 (14), 4252–4254. doi:10.1039/c1cc10631g

Chen, J., Kuriyama, N., Yuan, H., Takeshita, H. T., and Sakai, T. (2001). Electrochemical hydrogen storage in MoS_2 nanotubes. *J. Am. Chem. Soc.* 123 (47), 11813–11814. doi:10.1021/ja017121z

Chhowalla, M., and Amaratunga, G. A. J. (2000). Thin films of fullerene-like MoS_2 nanoparticles with ultra-low friction and wear. *Nature.* 407, 164–167. doi:10.1038/35025020

Feng, C., Ma, J., Li, H., Zeng, R., Guo, Z., and Liu, H. (2009). Synthesis of molybdenum disulfide (MoS_2) for lithium ion battery applications. *Mater. Res. Bull.* 44 (9), 1811–1815. doi:10.1016/j.materresbull.2009.05.018

Firmiano, E. G. S., Cordeiro, M. A. L., Rabelo, A. C., Dalmaschio, C. J., Pinheiro, A. N., Pereira, E. C., et al. (2012). Graphene oxide as a highly selective substrate to synthesize a layered MoS_2 hybrid electrocatalyst. *Chem. Commun.* 48 (62), 7687–7689. doi:10.1039/c2cc33397j

Firmiano, E. G. S., Rabelo, A. C., Dalmaschio, C. J., Pinheiro, A. N., Pereira, E. C., Schreiner, W. H., et al. (2014). Supercapacitor electrodes obtained by directly bonding 2D MoS_2 on reduced graphene oxide. *Advanced Energy Materials.* 4 (6), 1301380. doi:10.1002/aenm.201301380

Geim, A. K., and Grigorieva, I. V. (2013). Van der Waals heterostructures. *Nature.* 499, 419–425. doi:10.1038/nature12385

Ghosh, S., Barg, S., Jeong, S. M., and Ostrikov, K. (2020). Heteroatom-doped and oxygen-functionalized nanocarbons for high-performance supercapacitors. *Adv. Energy Mater.*, 10, 2001239. doi:10.1002/aenm.202001239

Ghosh, S., Sharath Kumar, J., Chandra Murmu, N., Sankar Ganesh, R., Inokawa, H., and Kuila, T. (2019). Development of carbon coated NiS_2 as positive electrode material for high performance asymmetric supercapacitor. *Compos. B Eng.* 177, 107373. doi:10.1016/j.compositesb.2019.107373

Gopalakrishnan, K., Sultan, S., Govindaraj, A., and Rao, C. N. R. (2015). Supercapacitors based on composites of PANI with nanosheets of nitrogen-doped RGO, BC 1.5 N, MoS 2 and WS 2. *Nanomater. Energy* 12, 52–58. doi:10.1016/j.nanoen.2014.12.005

Hao, C., Wen, F., Xiang, J., Wang, L., Hou, H., Su, Z., et al. (2014). Controlled incorporation of $Ni(OH)_2$ nanoplates into flowerlike MoS_2 nanosheets for flexible all-solid-state supercapacitors. *Adv. Funct. Mater.* 24 (42), 6700–6707. doi:10.1002/adfm.201401268

He, X., Bi, T., Zheng, X., Zhu, W., and Jiang, J. (2020). Nickel cobalt sulfide nanoparticles grown on titanium carbide MXenes for high-performance supercapacitor. *Electrochim. Acta.* 332, 135514. doi:10.1016/j.electacta.2019.135514

Hu, Z.-A., Xie, Y.-L., Wang, Y.-X., Xie, L.-J., Fu, G.-R., Jin, X.-Q., et al. (2009). Synthesis of α-cobalt hydroxides with different intercalated anions and effects of intercalated anions on their morphology, basal plane spacing, and capacitive property. *J. Phys. Chem. C.* 113 (28), 12502–12508. doi:10.1021/jp8106809

Huang, K.-J., Wang, L., Liu, Y.-J., Liu, Y.-M., Wang, H.-B., Gan, T., et al. (2013). Layered MoS_2-graphene composites for supercapacitor applications with enhanced capacitive performance. *Int. J. Hydrogen Energy.* 38 (32), 14027–14034. doi:10.1016/j.ijhydene.2013.08.112

Hwang, H., Kim, H., and Cho, J. (2011). MoS_2 nanoplates consisting of disordered graphene-like layers for high rate lithium battery anode materials. *Nano Lett.* 11 (11), 4826–4830. doi:10.1021/nl202675f

Jabeen, N., Hussain, A., Xia, Q., Sun, S., Zhu, J., and Xia, H. (2017). High-performance 2.6 V aqueous asymmetric supercapacitors based on in situ formed Na0.5 MnO_2 nanosheet assembled nanowall arrays. *Adv. Mater.* 29 (32), 1700804. doi:10.1002/adma.201700804

Ji, H., Liu, C., Wang, T., Chen, J., Mao, Z., Zhao, J., et al. (2015). Porous hybrid composites of few-layer MoS_2 nanosheets embedded in a carbon matrix with an excellent supercapacitor electrode performance. *Small.* 11 (48), 6480–6490. doi:10.1002/smll.201502355

Jiang, Q., Kurra, N., Alhabeb, M., Gogotsi, Y., and Alshareef, H. N. (2018). All pseudocapacitive MXene-RuO_2 asymmetric supercapacitors. *Adv. Energy Mater.* 8 (13), 1703043. doi:10.1002/aenm.201703043

Khan, M. Z., Gul, I. H., Baig, M. M., and Khan, A. N. (2020). Comprehensive study on structural, electrical, magnetic and photocatalytic degradation properties of Al^{3+} ions substituted nickel ferrites nanoparticles. *J. Alloys Compd.* 848, 155795. doi:10.1016/j.jallcom.2020.155795

Kim, B. K., Chabot, V., and Yu, A. (2013). Carbon nanomaterials supported $Ni(OH)_2$/NiO hybrid flower structure for supercapacitor. *Electrochim. Acta.* 109, 370–380. doi:10.1016/j.electacta.2013.07.119

Kulkarni, S. B., Patil, U. M., Shackery, I., Sohn, J. S., Lee, S., Park, B., et al. (2014). High-performance supercapacitor electrode based on a polyaniline nanofibers/3D graphene framework as an efficient charge transporter. *J. Mater. Chem.* 2 (14), 4989–4998. doi:10.1039/c3ta14959e

Lee, Y.-H., Zhang, X.-Q., Zhang, W., Chang, M.-T., Lin, C.-T., Chang, K.-D., et al. (2012). Synthesis of large-area MoS_2 atomic layers with chemical vapor deposition. *Adv. Mater.* 24 (17), 2320–2325. doi:10.1002/adma.201104798

Li, H., Jiang, N., Deng, Q., and Wang, X. (2019a). Vertically MoS_2 on reduced graphene oxide with superior durability for quasi-solid-state supercapacitor. *Chemistry.* 4 (43), 12815–12823. doi:10.1002/slct.201903517

Li, H., Wang, S., Feng, M., Yang, J., and Zhang, B. (2019b). MOF-derived $ZnCo_2O_4$/C wrapped on carbon fiber as anode materials for structural lithium-ion batteries. *Chin. Chem. Lett.* 30, 529–532. doi:10.1016/j.cclet.2018.06.024

Li, Y., Wang, H., Xie, L., Liang, Y., Hong, G., and Dai, H. (2011). MoS_2 nanoparticles grown on graphene: an advanced catalyst for the hydrogen evolution reaction. *J. Am. Chem. Soc.* 133 (19), 7296–7299. doi:10.1021/ja201269b

Liu, S., Yin, Y., Hui, K. S., Hui, K. N., Lee, S. C., and Jun, S. C. (2018a). High-performance flexible quasi-solid-state supercapacitors realized by molybdenum dioxide@nitrogen-doped carbon and copper cobalt sulfide tubular nanostructures. *Adv. Sci.* 5 (10), 1800733. doi:10.1002/advs.201800733

Liu, S., Yin, Y., Wu, M., Hui, K. S., Hui, K. N., Ouyang, C.-Y., et al. (2018b). Phosphorus-mediated MoS_2 nanowires as a high-performance electrode material for quasi-solid-state sodium-ion intercalation supercapacitors. *Small.* 15 (4), 1803984. doi:10.1002/smll.201803984

Lv, M., Fan, F., Pan, L., Shen, H., Pervaiz, E., Wang, J., et al. (2019). Molten salts-assisted fabrication of Fe, S, and N Co-doped carbon as efficient oxygen reduction reaction catalyst. *Energy Technol.* 8 (1), 1900896. doi:10.1002/ente.201900896

Lv, T., Yao, Y., Li, N., and Chen, T. (2016). Highly stretchable supercapacitors based on aligned carbon nanotube/molybdenum disulfide composites. *Angew. Chem. Int. Ed.* 55 (32), 9191–9195. doi:10.1002/anie.201603356

Ma, G., Peng, H., Mu, J., Huang, H., Zhou, X., and Lei, Z. (2013). *In situ* intercalative polymerization of pyrrole in graphene analogue of MoS_2 as advanced electrode material in supercapacitor. *J. Power Sources.* 229, 72–78. doi:10.1016/j.jpowsour.2012.11.088

Matte, H. S., Gomathi, A., Manna, A. K., Late, D. J., Datta, R., Pati, S. K., et al. (2010). MoS_2 and WS_2 analogues of graphene. *Angew Chem. Int. Ed. Engl.* 49 (24), 4059–4062. doi:10.1002/anie.201000009

Mehran, T., and Baig, M. M. (2019). "Metal sulfide/mxene based nanostructured electrode materials for high-performance supercapacitors," in Electrochemical conference on energy and the environment (ECEE 2019): bioelectrochemistry and energy storage, Glasgow, Scotland, July 21–26, 2019.

Miao, Y., Sui, Y., Zhang, D., Qi, J., Wei, F., Meng, Q., et al. (2019). Polyhedral $NiCoSe_2$ synthesized via selenization of metal-organic framework for supercapacitors. *Mater. Lett.* 242, 42–46. doi:10.1016/j.matlet.2019.01.096

Molina-Sánchez, A., Hummer, K., and Wirtz, L. (2015). Vibrational and optical properties of MoS 2 : from monolayer to bulk. *Surf. Sci. Rep.* 70 (4), 554–586. doi:10.1016/j.surfrep.2015.10.001

Murugan, A. V., Quintin, M., Delville, M.-H., Campet, G., Gopinath, C. S., and Vijayamohanan, K. (2006). Exfoliation-induced nanoribbon formation of poly(3,4-ethylene dioxythiophene) PEDOT between MoS_2 layers as cathode material for lithium batteries. *J. Power Sources.* 156 (2), 615–619. doi:10.1016/j.jpowsour.2005.06.022

Muthu, N. S., and Gopalan, M. (2019). Mesoporous nickel sulphide nanostructures for enhanced supercapacitor performance. *Appl. Surf. Sci.* 480, 186–198. doi:10.1016/j.apsusc.2019.02.250

Nagaraju, G., Tharamani, C. N., Chandrappa, G. T., and Livage, J. (2007). Hydrothermal synthesis of amorphous MoS_2 nanofiber bundles via acidification of ammonium heptamolybdate tetrahydrate. *Nanoscale Res. Lett.* 2, 461. doi:10.1007/s11671-007-9087-z

Raghu, M. S., Yogesh Kumar, K., Rao, S., Aravinda, T., Sharma, S. C., and Prashanth, M. K. (2018). Simple fabrication of reduced graphene oxide -few layer MoS_2 nanocomposite for enhanced electrochemical performance in supercapacitors and water purification. *Phys. B Condens. Matter.* 537, 336–345. doi:10.1016/j.physb.2018.02.017

Rani, B. J., Pradeepa, S. S., Hasan, Z. M., Ravi, G., Yuvakkumar, R., and Hong, S. I. (2020). Supercapacitor and OER activity of transition metal (Mo, Co, Cu) sulphides. *J. Phys. Chem. Solid.* 138, 109240. doi:10.1016/j.jpcs.2019.109240

Rapoport, L., Fleischer, N., and Tenne, R. (2005). Applications of $WS_2(MoS_2)$ inorganic nanotubes and fullerene-like nanoparticles for solid lubrication and for structural nanocomposites. *J. Mater. Chem.* 15 (18), 1782–1788. doi:10.1039/b417488g

Rathinamala, I., Babu, I. M., William, J. J., Muralidharan, G., and Prithivikumaran, N. (2020). CdS microspheres as promising electrode materials for high performance supercapacitors. *Mater. Sci. Semicond. Process.* 105, 104677. doi:10.1016/j.mssp.2019.104677

Rosentsveig, R., Margolin, A., Gorodnev, A., Popovitz-Biro, R., Feldman, Y., Rapoport, L., et al. (2001). Synthesis of fullerene-like MoS_2 nanoparticles and their tribological behavior. *J. Mater. Chem.* 19 (25), 4368–4374. doi:10.1039/B820927H

Sadan, M. B., Houben, L., Enyashin, A. N., Seifert, G., and Tenne, R. (2008). Atom by atom: HRTEM insights into inorganic nanotubes and fullerene-like structures. *Proc. Natl. Acad. Sci. Unit. States Am.* 105 (41), 15643–15648. doi:10.1073/pnas.0805407105

Sarkar, A., Chakraborty, A. K., and Bera, S. (2018). NiS/rGO nanohybrid: an excellent counter electrode for dye sensitized solar cell. *Sol. Energy Mater. Sol. Cell.* 182, 314–320. doi:10.1016/j.solmat.2018.03.026

Sha, C., Lu, B., Mao, H., Cheng, J., Pan, X., Lu, J., et al. (2016). 3D ternary nanocomposites of molybdenum disulfide/polyaniline/reduced graphene oxide aerogel for high performance supercapacitors. *Carbon.* 99, 26–34. doi:10.1016/j.carbon.2015.11.066

Shaw, J. C., Zhou, H., Chen, Y., Weiss, N. O., Liu, Y., Huang, Y., et al. (2014). Chemical vapor deposition growth of monolayer MoSe2 nanosheets. *Nano Res.* 7, 511–517. doi:10.1007/s12274-014-0417-z

Soon, J. M., and Loh, K. P. (2007). Electrochemical double-layer capacitance of MoS_2 nanowall films. *Electrochem. Solid State Lett.* 10 (11), 250–254. doi:10.1149/1.2778851

Sun, G., Zhang, X., Lin, R., Yang, J., Zhang, H., and Chen, P. (2015). Hybrid fibers made of molybdenum disulfide, reduced graphene oxide, and multi-walled carbon nanotubes for solid-state, flexible, asymmetric supercapacitors. *Angew. Chem. Int. Ed.* 54 (15), 4651–4656. doi:10.1002/anie.201411533

Sun, H., Liu, H., Hou, Z., Zhou, R., Liu, X., and Wang, J.-G. (2020). Edge-terminated MoS_2 nanosheets with an expanded interlayer spacing on graphene to boost supercapacitive performance. *Chem. Eng. J.* 387, 124204. doi:10.1016/j.cej.2020.124204

Sun, M., Adjaye, J., and Nelson, A. E. (2004). Theoretical investigations of the structures and properties of molybdenum-based sulfide catalysts. *Appl. Catal. Gen.* 263 (2), 131–143. doi:10.1016/j.apcata.2003.12.011

Sun, P., Zhang, W., Hu, X., Yuan, L., and Huang, Y. (2014). Synthesis of hierarchical MoS_2 and its electrochemical performance as an anode material for lithium-ion batteries. *J. Mater. Chem.* 2 (10), 3498–3504. doi:10.1039/c3ta13994h

Sun, T., Li, Z., Liu, X., Ma, L., Wang, J., and Yang, S. (2016). Facile construction of 3D graphene/MoS_2 composites as advanced electrode materials for supercapacitors. *J. Power Sources.* 331, 180–188. doi:10.1016/j.jpowsour.2016.09.036

Tang, H., Wang, J., Yin, H., Zhao, H., Wang, D., and Tang, Z. (2015). Growth of polypyrrole ultrathin films on MoS_2 monolayers as high-performance supercapacitor electrodes. *Adv. Mater.* 27 (6), 1117–1123. doi:10.1002/adma.201404622

Tian, Y., Song, X., Liu, J., Zhao, L., Zhang, P., and Gao, L. (2019). Generation of monolayer MoS_2 with 1T phase by spatial-confinement-induced ultrathin PPy anchoring for high-performance supercapacitor. *Adv. Mater. Interfaces.* 6 (10), 1900162. doi:10.1002/admi.201900162

Vikraman, D., Karuppasamy, K., Hussain, S., Kathalingam, A., Sanmugam, A., Jung, J., et al. (2019). One-pot facile methodology to synthesize MoS_2-graphene hybrid nanocomposites for supercapacitors with improved electrochemical capacitance. *Compos. B Eng.* 161, 555–563. doi:10.1016/j.compositesb.2018.12.143

Wang, B., Cheng, Y., Su, H., Cheng, M., Li, Y., Geng, H., et al. (2020a). Boosting transport kinetics of cobalt sulfides yolk–shell spheres by anion doping for advanced lithium and sodium storage. *ChemSusChem.* 13 (16), 4078–4085. doi:10.1002/cssc.202001261

Wang, M. Y., Guo, J. Z., Wang, Z. W., Gu, Z. Y., Nie, X. J., Yang, X., et al. (2020b). Isostructural and multivalent anion substitution toward improved phosphate cathode materials for sodium-ion batteries. *Small.* 16 (16), 1907645. doi:10.1002/smll.201907645

Wang, Q. H., Kalantar-Zadeh, K., Kis, A., Coleman, J. N., and Strano, M. S. (2012). Electronics and optoelectronics of two-dimensional transition metal dichalcogenides. *Nat. Nanotechnol.* 7, 699–712. doi:10.1038/nnano.2012.193

Wang, Y.-Y., Hou, B.-H., Guo, J.-Z., Ning, Q.-L., Pang, W.-L., Wang, J., et al. (2018). An ultralong lifespan and low-temperature workable sodium-ion full battery for stationary energy storage. *Adv. Energy Mater.* 8 (18), 1703252. doi:10.1002/aenm.201703252

Wei, S., Zhou, R., and Wang, G. (2019). Enhanced electrochemical performance of self-assembled nanoflowers of MoS_2 nanosheets as supercapacitor electrode materials. *ACS Omega.* 4 (14), 15780–15788. doi:10.1021/acsomega.9b01058

Winter, M., and Brodd, R. J. (2004). What are batteries, fuel cells, and supercapacitors? *Chem. Rev.* 104 (10), 4245–4270. doi:10.1021/cr020730k

Xiao, W., Zhou, W., Feng, T., Zhang, Y., Liu, H., and Tian, L. (2016). Simple synthesis of molybdenum disulfide/reduced graphene oxide composite hollow microspheres as supercapacitor electrode material. *Materials.* 9 (9), 783. doi:10.3390/ma9090783

Xu, J.-M., Wang, X.-C., and Cheng, J.-P. (2020). Supercapacitive performances of ternary $CuCo_2S_4$ sulfides. *ACS Omega.* 5 (3), 1305–1311. doi:10.1021/acsomega.9b03865

Xu, Y., Bai, H., Lu, G., Li, C., and Shi, G. (2008). Flexible graphene films via the filtration of water-soluble noncovalent functionalized graphene sheets. *J. Am. Chem. Soc.* 130 (18), 5856–5857. doi:10.1021/ja800745y

Yan, J., Ren, C. E., Maleski, K., Hatter, C. B., Anasori, B., Urbankowski, P., et al. (2017). Flexible MXene/graphene films for ultrafast supercapacitors with

outstanding volumetric capacitance. *Adv. Funct. Mater.* 27 (30), 1701264. doi:10.1002/adfm.201701264

Yang, W., Guo, H., Yue, L., Li, Q., Xu, M., Zhang, L., et al. (2020). Metal-organic frameworks derived MMoSx (M = Ni, Co and Ni/Co) composites as electrode materials for supercapacitor. *J. Alloys Compd.* 834, 154118. doi:10.1016/j.jallcom.2020.154118

Zhang, X., Huang, X., Xue, M., Ye, X., Lei, W., Tang, H., et al. (2015). Hydrothermal synthesis and characterization of 3D flower-like MoS_2 microspheres. *Mater. Lett.* 148, 67–70. doi:10.1016/j.matlet.2015.02.027

Zhao, G., Cheng, Y., Sun, P., Ma, W., Hao, S., Wang, X., et al. (2020). Biocarbon based template synthesis of uniform lamellar MoS_2 nanoflowers with excellent energy storage performance in lithium-ion battery and supercapacitors. *Electrochim. Acta.* 331, 135262. doi:10.1016/j.electacta.2019.135262

Zhao, G., Hao, S., Guo, J., Xing, Y., Zhang, L., and Xu, X. (2021). Design of p-n homojunctions in metal-free carbon nitride photocatalyst for overall water splitting. *Chin. J. Catal.* 42 (3), 501–509. doi:10.1016/s1872-2067(20)63670-1

Zhao, J., Li, Z., Yuan, X., Yang, Z., Zhang, M., Meng, A., et al. (2018). A high-energy density asymmetric supercapacitor based on Fe_2O_3 nanoneedle arrays and $NiCo_2O_4$/$Ni(OH)_2$ hybrid nanosheet arrays grown on SiC nanowire networks as free-standing advanced electrodes. *Adv. Energy Mater.* 8 (12), 1702787. doi:10.1002/aenm.201702787

Zhao, T., Peng, X., Zhao, X., Hu, J., Jiang, T., Lu, X., et al. (2020). Preparation and performance of carbon dot decorated copper sulphide/carbon nanotubes hybrid composite as supercapacitor electrode materials. *J. Alloys Compd.* 817, 153057. doi:10.1016/j.jallcom.2019.153057

Zhou, K.-G., Mao, N.-N., Wang, H.-X., Peng, Y., and Zhang, H.-L. (2011). A mixed-solvent strategy for efficient exfoliation of inorganic graphene analogues. *Angew. Chem. Int. Ed.* 50 (46), 10839–10842. doi:10.1002/anie.201105364

Zhu, J., Sharma, Y. K., Zeng, Z., Zhang, X., Srinivasan, M., Mhaisalkar, S., et al. (2011). Cobalt oxide nanowall arrays on reduced graphene oxide sheets with controlled phase, grain size, and porosity for Li-ion battery electrodes. *J. Phys. Chem. C.* 115 (16), 8400–8406. doi:10.1021/jp2002113

Conflict of Interest: The authors declare that the research was conducted in the absence of any commercial or financial relationships that could be construed as a potential conflict of interest.